Flux Qubits and Coherent Tunable Couplings between Them

Zheng Li[1]

[1]*Department of Electrical and Computer Engineering,*

Rice University, Houston, Texas, 77005, USA

(Dated: December 17, 2009)

Abstract

Flux qubits (also known as persistent current qubits), one kind of superconducting tunnel junction circuits, are recently demonstrated as a promising candidate to realize quantum computations. In order to do large-scale quantum information processing, it is necessary to switch on and off the couplings between individual flux qubits in the time-domain while those qubits retain coherence. This report contains two parts: one is to describe my understanding of models, fabrications and measurements for one single flux qubit; the other is to compare two proposed schemes and the corresponding experimental realizations of coherent tunable couplings between flux qubits.

I. INTRODUCTION

Flux qubit consists of a superconducting loop interrupted by a number of Josephson tunnel junctions. Compared to other types of superconducting qubits such as "charge qubit" ("cooper-pair-box" qubit)[1,2], it possesses relatively larger Josephson junctions and the "bit" is represented by two persistent currents of opposite directions circulating in its loop when an external flux applied to the loop is close to a half integer number of flux quanta $\Phi_0 = h/2e$. Since proposed in Ref. 3, flux qubits have been explored both theoretically and experimentally so much in various aspects for finding possible implementation of a quantum computer in the past decade.[4–15] This article is organized as follows. First, I give a theoretical description of one single flux qubit and a short review on how it is fabricated and measured; then, I discuss and compare two tunable coupling schemes and their experimental realizations; finally, I present a conclusion of my understanding of flux qubit.

II. SINGLE FLUX QUBIT

A. model

Diving into the details of Ref. 3, I first summarize the authors' research method here. The inventors of flux qubits do not explore further why and how we can model an single superconducting circuit element in the view of materials or other related regions; instead, they abstract the corresponding 2-port circuit model for each element to design mesoscopic superconducting circuits in a higher level. They utilize a standard quantization procedure to obtain the Hamiltonian for the corresponding quantum system that, in short, the flux and the charge stand as a pair of conjugate operators for the circuit as an analogy to the position $\vec{x}$ and the momentum $\vec{p}$ of particles moving in a given potential. After analyzing the circuit and its Hamiltonian they found useful parameters to simplify the complex quantum system into a simple two-level one. I only discuss the latter system in this article.

Flux qubit's circuit model is shown in fig. 1(a). In the classical DC regime, when the external flux $\Phi_{ext} = \Phi_0 f$ is biased at close proximity of a degenerate point $f = 0.5$, as a mechanic analogy[5], the system behaves as one particle in a double-well potential shown in 1(b). At a classical limitation, the particle only pins in the bottoms of the well. Those two classical states have a well-defined characteristics: due to the external flux, they corre-

spond to persistent currents of opposite signs in the loop (clockwise or counterclockwise). However, in quantum mechanics, those two classical states should spread a little due to the Heisenberg uncertainty principle and couple with each other through a tunneling Δ between the barrier. The bottoms of the potential can also be altered by Φ_{ext} with energy $\pm\frac{1}{2}\epsilon = \pm I_p(\Phi - \Phi_0/2)$ because of persistent currents of opposite signs in the loop. The Hamiltonian $\hat{H}_{qb} = -\frac{1}{2}(\Delta\sigma_x + \epsilon\sigma_z)$ describes this system on the basis of the persistent current states $|\uparrow\rangle$ and $|\downarrow\rangle$, where $\sigma_{x,y,z}$ are Pauli matrices. The loop current operator is $\hat{I}_q = I_p\sigma_z$. Define that $\hat{H}_{qb}$ has its eigen-states $|\ 0\rangle$ and $|\ 1\rangle$ with eigen-energy E_0 and E_1 ($E_0 < E_1$). When $f = 0.5$, eigen-states $|\ 0\rangle = \frac{|\uparrow\rangle+|\downarrow\rangle}{\sqrt{2}}$ and $|\ 1\rangle = \frac{|\uparrow\rangle-|\downarrow\rangle}{\sqrt{2}}$ are solved as symmetrical and anti-symmetrical superpositions of $|\uparrow\rangle$ and $|\downarrow\rangle$, with loop current expectation values $\langle\hat{I}_q\rangle = 0$. When $|f - 0.5|$ increases and, thus, $E_1 - E_0 = \omega = \sqrt{\Delta^2 + \epsilon^2}$ increases, the superpositions of the eigen states decrease, and finally, they become $|\uparrow\rangle$ and $|\downarrow\rangle$, respectively. See fig. 1(c).

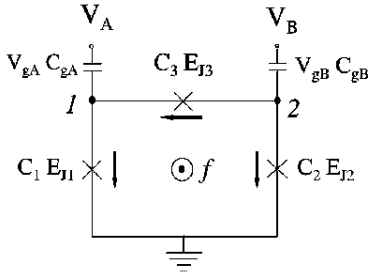

(a)Circuit model

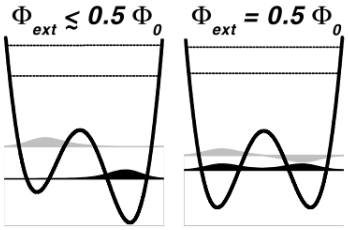

(b)double-well potential

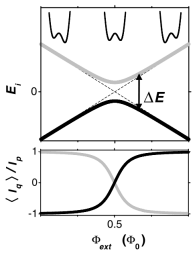

(c)two-level system

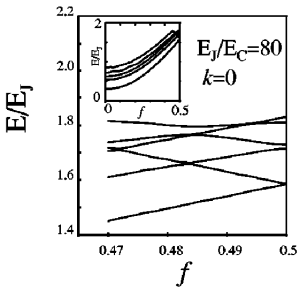

(d)Energy band diagram

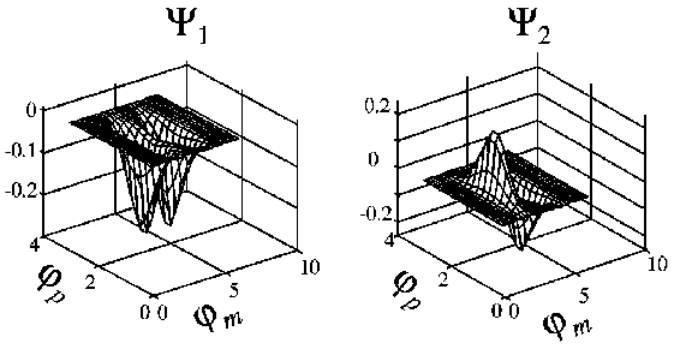

(e)Eigen-functions at the degenerate point

FIG. 1: Properties of a single flux qubit, modified from Refs. 3 and 5. Notes: the sub-figure (c) shows the two-level system's band structure and the corresponding loop current expectation values of eigen-states.

The above explanation is relatively intuitive but not restrict. At least the words in Ref. 5 lead me to a wrong understanding that I_p can be obtained in the classical regime. Therefore, I emphasize two complementary points here: the two-level system assumption is based on the well separation of the corresponding states from other quantum states, see the whole energy diagram of one flux qubit in fig. 1(d); one flux qubit is a mesoscopic quantum system, unlike the intrinsic spins of electrons, the states $|\uparrow\rangle$ and $|\downarrow\rangle$ have their own distributions in the phase space (φ_m, φ_p) as $\frac{\Psi_1 \pm \Psi_2}{\sqrt{2}}$, with $I_p = \langle j \mid \hat{I}_q \mid j \rangle_{j=\uparrow,\downarrow}$.

One notable thing is that $\Phi_{ext} = \frac{1}{2}\Phi_0$ is called the optimal point where flux qubit has a longer dephasing time.[9,10,13] I give my opinion which may be "naive". Low frequency noises $\delta\Phi(t)$ can impact the coherent evolution of one state of flux qubit, e.g., $\mid e(t)\rangle = a \mid 0(t)\rangle + be^{i\phi(t)} \mid 1(t)\rangle$. Because the noises only affect $\mid e(t)\rangle$ slowly, no excitation occurs between $\mid 0(t)\rangle$ and $\mid 1(t)\rangle$, $\mid e(t)\rangle$ evolves in the basis of $\mid 0(t)\rangle$ and $\mid 1(t)\rangle$, but the phase varies as $\phi(t) = \int_0^t \omega(t_0)dt_0/\hbar$, known as an adiabatic assumption. If $\frac{\partial\omega}{\partial\Phi_{ext}} = 0$, then $\phi(t)$ is insensitive to $\delta\Phi_{ext}(t)$ to the first order, thus reducing the dephasing effects. Since the tunneling part Δ almost depends on the shapes of $\Psi_{1,2}$ and the barriers between $|\uparrow\rangle$ and $|\downarrow\rangle$, yielding $\frac{\partial\Delta}{\partial\Phi_{ext}} = 0$, $\frac{\partial\omega}{\partial\Phi_{ext}} = 0$ requires $\epsilon = 0$ as the optimal point.

B. fabrications

Superconducting circuits for quantum computations including flux qubits can be fabricated using silicon-compatible techniques: to utilize electron beam lithography to define masks, two-angle shadow evaporations of metals such as Aluminium with a specific oxidation procedure between them to form Josephson junctions and other shadow evaporations to obtain other metal layers. Optimizing recipes for those techniques is fundamental to fabricate good devices. The scaning electron graph (SEM) of charge and flux qubits fabricated in different groups are shown in fig. 2. Figures 2(a), 2(c) and 2(d) clearly reveal typical devices employing shadow evaporations, where the repeated and overlapping patterns refer to evaporations using the same mask. Figures 2(b), 2(c) and 2(d) show different patterns to realize one flux qubit. This kind of diversity also indicates the high flexibility of designing superconducting circuits.

Electron beam lithography and that all of devices are fabricated in the same situation in one chip is one of the advantages of the superconducting circuits. It is reported that there

is only 0.5% difference between the loop sizes of two flux qubits.[15] However, one exceptions may be the sizes of Josephson junctions because those junctions are formed using metal wire edges of not good shapes (See fig. 2(c)), although the thickness of the oxidation layers of Josephson junctions is relatively easier to control.

It is also found from the SEM pictures that the auxiliary circuits are also fabricated with qubits, e.g., a DC superconducting quantum interference device (SQUID)[17] for measurements, additional DC bias and microwave signal wires. Wisely arranging those undetachable parts with flux qubits, however, makes the circuit designs more complicated. For instance, different arrangements may lead to completely different mutual inductance distributions; the circuits fabricated should be isolated from surrounding enviroment noises normally while it can also be switched into a readout state which, of course, is coupled back to the environments.

C. measurements

Flux qubits' resonant frequencies are generally on the order of $1 \sim 10$GHz. Therefore, the circuits should be maintained in a dilution refrigerator in a very low temperature of the order of $10mK$ while auxiliary circuits amplify the signals step by step from $\sim 10mK$ to the room temperature for finally reading-out. Most of the final measured results are related to the possibilities of specific events, so the measuring circuits are also designed to repeat the experiments automatically thousand to million times.

One measuring technique is to utilize a DC-SQUID as a magnetometer to detect the loop current of flux qubit shown in fig.3. If the bias current I_b is turned on to reach the critical current point for DC-SQUID, it is crucial that the additional flux in the loop of DC-SQUID contributed by the loop current of the flux qubit via the mutual inductance: the circulating current can increase or decrease (determined by its direction) the possibility of the event that DC-SQUID is switched into a voltage state and outputs a non-zero V_{out}. The possibilities can be measured if we repeat the experiment multi-times.

One interesting thing is that I_b also changes the circulating current in the loop of DC-SQUID, especially, when those two junctions of DC-SQUID differ from each other, which impose a small additional flux (the phase $\Delta\gamma_q$) to the flux qubit via the mutual inductance. Therefore Ref. 6 shown in fig. 3 employs a good measurement scheme: when the flux qubit

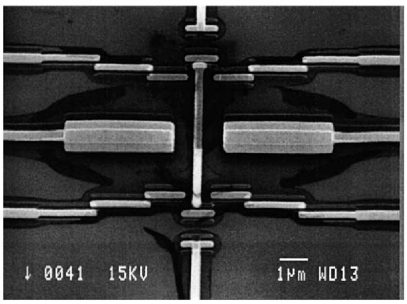

(a)Ref. 1

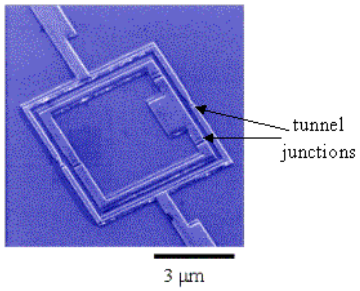

(b)Ref. 4,16

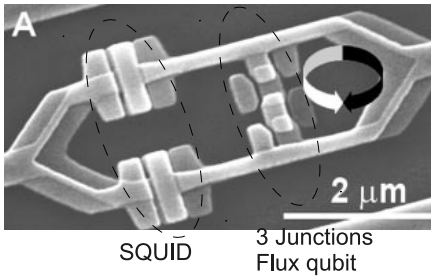

(c)Ref. 6

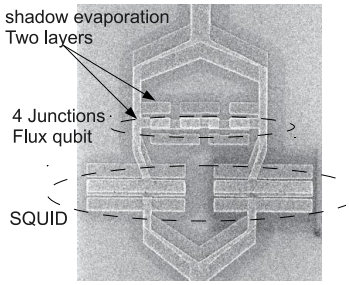

(d)Ref. 13

FIG. 2: SEM pictures of qubit systems, slightly modified from the original papers (see the sub-captions). (a), one charge qubit without loops ; (b) the inner loop is flux qubit while the outer one DC-SQUID; (c) 3-junction flux qubit shared its loop with one DC-SQUID, dashed line indicates the two junctions of the DC-SQUID; (d) 4-junction flux qubit shared its loop with one DC-SQUID, dashed line indicates the two junctions of the DC-SQUID.

is not required to measure, we can turn on a slight(ideally zero) I_b to make sure that the flux qubit runs at the optimal point with zero average loop current; when we want to measure it, a large I_b drives the flux qubit into a non-optimal point where its two eigen-states have larger average loop currents.

III. TUNABLE COUPLING BETWEEN FLUX QUBITS

A. theoretical schemes

Two flux qubits, e.g., the kth and lth ones, can couple with each other via their mutual inductance M_{kl}. Analogy to the spin coupling, the coupling operator can be expressed as $M_{kl}\hat{I}_{qk}\hat{I}_{ql} = J_{kl}\sigma_z^k\sigma_z^l$ with $J_{kj} = M_{kj}I_{pk}I_{pj}$. One interesting thing is that in the above

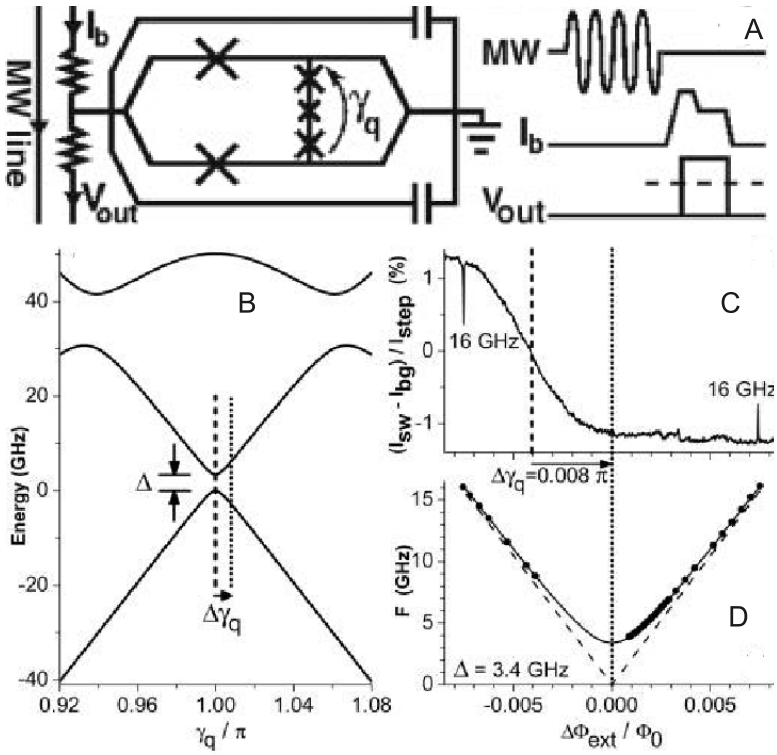

FIG. 3: Demonstrations of measuring setups.[6] (A) Basic circuit model, "MW" means microwave signals, I_b is the bias current of the DC-SQUID, V_{out} will have a non-zero output if DC-SQUID is switched into a voltage-state; (B) Band structures of flux qubit, a large I_b leads to $\Delta\gamma_q$; (C) Difference in percents of effective switching current of DC-SQUID due to the different loop currents of the ground state of flux qubit at different Φ_{ext}. See the bias effect caused by $\Delta\gamma_q$ indicated by the dashed line: if $\Delta\gamma_q = 0$, when $\Delta\Phi = 0$, the result should be zero in percent because the ground state possesses a zero average loop current; (D) Resonant spectra as a function of the microwave signal F and the external flux bias $\Delta\Phi_{ext}$.

derivations the authors in Ref. 3 construct the Hamiltonian without considering the loop's self-inductance, the size of which should be of the same order of the mutual inductance. It is acceptable in this application in my opinion. Along the loop the self-inductance is connected to those Josephson junctions in series. Since the Josephson junctions, due to their large sizes, can provide much large effective inductances, the self-inductance should be neglected approximately. However, for the coupling between different flux qubits, the mutual inductances become crucial because of lacking other stronger coupling between them. It is

expected that this kind of coupling is relatively weak; however, the small loop size can also reduce the noises coming from the environment: there exists a trade-off between them.

I select Ref. 7,11 and 14 to understand how the tunable coupling scheme works. Two coupling schemes are presented in fig. 4: coupling two flux qubits via DC-SQUID or a third flux qubit.

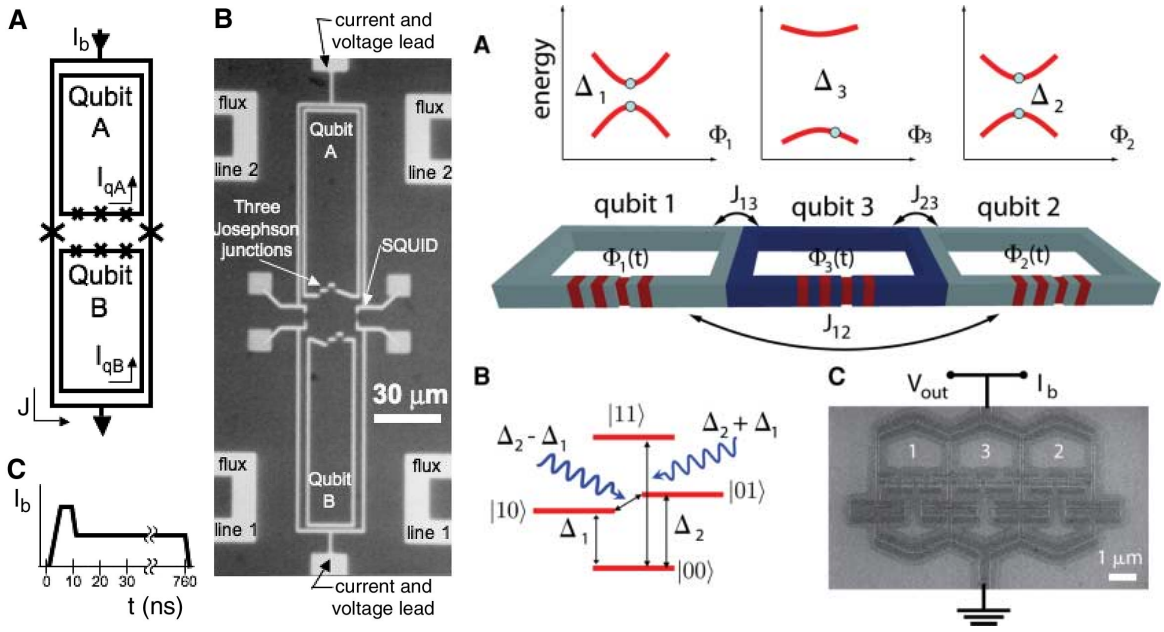

(a)via DC-SQUID (b)via a third-qubit

FIG. 4: Two tunable coupling schemes and their realizations, modified from Refs. 12 and 15, respectively.

The authors[14] proposed a scheme that qubit 1 is coupled with qubit 2 via a third adiabatic qubit, qubit 3. Qubit 3 possesses a higher Δ_3 than those two others. It is not difficult to write down its Hamiltonian

$$\hat{H}_{3q} = \hat{H}_{dc} + \hat{H}_{3MW} \tag{1}$$

$$\hat{H}_{3dc} = -\frac{1}{2}\sum_{j=1}^{3}(\Delta_j\sigma_x^j + \epsilon_j\sigma_z^j) - \sum_{k\neq l} J_{kl}\sigma_z^k\sigma_z^l \tag{2}$$

$$\hat{H}_{3MW} = -\frac{1}{2}\sum_{j=1}^{3}\delta\epsilon_j(t)\sigma_z^j \tag{3}$$

where besides the DC part $\hat{H}_{3dc}$ we also apply independent microwave signals $\delta\epsilon_j(t) = 2I_{pj}\delta\Phi_j(t)$ to flux qubits via the external flux biases.

As we known[11], three individual subspaces of those three flux qubits $\{|\ 0_j\rangle, |\ 1_j\rangle\}$ span a Hilbert space $\{|\ i_1, j_2, k_3\rangle\}\,|_{i,j,k=0,1}$, where $\hat{H}_{3q}$ can be expressed as a 8×8 matrix. For a given time t, we can choose another matrix $\hat{U}(t)$ and diagonalize the 8×8 matrix $\hat{H}_{3q}$ as $\hat{U}\hat{H}_{3q}\hat{U}^{\dagger} = \hat{H}_{2q}^{eff}\ |\ 0_3(t)\rangle\langle 0_3(t)\ | + \hat{H}_{2q}^{ex}\ |\ 1_3(t)\rangle\langle 1_3(t)\ |$ for qubit 3. Since qubit 3 with $|\omega_3(t)| \gg |\omega_{1,2}(t)|$ is frozen in its ground state and operated adiabatically, only $\hat{H}_{2q}^{eff}$ dominates in the dynamics of qubits 1 and 2. The authors in Ref. 14 present such a way to solve the diagonalization problem using a perturbation method, the Schrieffer-Wolff transformation. As a hint here I assume there exists only one state in the system of qubits 1 and 2 coupling with qubit 3. Then we have a 2×2 matrix $\hat{H}_{2\times 2} = -\frac{1}{2}(\omega_3\sigma_z + \Delta_{tmp}\sigma_x)$. As shown in the previous discussions on the self and mutual inductances, we have the mutual inductive energy $\Delta_{tmp} \ll \omega_3$ and the corresponding $\hat{H}_{2q}^{eff}$ becomes a number as $H_{tmp}^{eff} = -\frac{1}{2}\sqrt{\omega_3^2 + \Delta_{tmp}^2} \simeq -\frac{1}{2}\omega_3 - \frac{\Delta_{tmp}^2}{4\omega_3}$. This number indicates that besides the original zero-point energy $-\frac{1}{2}\omega_3$ for qubit 3 a correction is also included where a minus sign means that the coupling lowers the total energy because qubit 3 stays in its the ground states. Back to $\hat{H}_{2q}^{eff}$, its form reads in a similar style as

$$\hat{H}_{2q}^{eff} \ = \ -\frac{1}{2}\sum_{j=1}^{2}(\Delta_j^{eff}\sigma_x^j + \epsilon_j^{eff}\sigma_z^j) - J_{12}^{eff}(t)\sigma_z^1\sigma_z^2 - \frac{1}{2}\sum_{j=1}^{2}\delta\epsilon_j(t)\sigma_z^j, \tag{4}$$

where

$$\epsilon_j^{eff} \ = \ \epsilon_j + \frac{2\epsilon_3(t)J_{j3}}{\omega_3(t)} = \epsilon_j - 2M_{j3}I_{pj}\langle 0_3\ |\ \hat{I}_{q3}\ |\ 0_3\rangle \tag{5}$$

$$\Delta_j^{eff} \ = \ \Delta_j - \frac{2(J_{j3}\Delta_3)^2\Delta_j}{\omega_3(t)^2[\omega_3(t)^2 - \Delta_j^2 - \epsilon_j^2]} \tag{6}$$

$$J_{12}^{eff} \ \simeq \ \left(M_{12} - \frac{M_{13}M_{23}}{L_Q(t)}\right)I_{p1}I_{p2} = J_{12} + \frac{2J_{23}J_{13}\Delta_3^2}{\omega_3(t)^3}, \tag{7}$$

$$L_Q^{-1}(t) \ = \ \frac{\partial\langle 0_3\ |\ \hat{I_{q3}}\ |\ 0_3\rangle}{\partial\Phi_3} = -\frac{2I_{p3}^2\Delta_3^2}{\omega_3(t)^3}. \tag{8}$$

Comments are presented here: 1) $\omega_3(t)$ as a divider makes all of the corrections as perturbations; 2) the loop current of the ground state of qubit 3 lower ϵ_j to ϵ_j^{eff} through the mutual inductance; 3) $J_{12}^{eff}(t)$ tells us that the auxiliary qubit 3 indirectly connects qubits 1 and 2 using its own flux response to qubits 1 and 2 via the mutual inductances; 4) AC components of qubit 3 are also neglected.

For point 3), I would like to give the explanations in Ref. 7. If qubit 2 switches the current, it apply a small flux change $\delta\Phi_3 = 2M_{23}I_{p2}$ to qubit 3; due to the adiabatic assumption qubit 3 is still frozen in the ground state but with a change in its loop current $\Delta I_J =$

$\delta\Phi_3/L_Q(t)$, and, finally, the mutual inductance M_{13} shifts the energy of qubit 1 with $K_s = -2M_{13}M_{23}I_{p1}I_{p2}/L_Q(t)$. Here the energy "flows"along a coupling chain from qubit 2 to qubit 1. Again the issue about the self and mutual-inductances rises: each qubit has no feed back during our analysis even though it has its self-inductance, which also suggests that the term $J_{12}^{eff}(t)$ only approximates the rigorous but much complex one in lower orders. The idea of the DC-SQUID coupling scheme[7] does not differ from this scheme in this context. What differs is that they apply a large I_b to generate a proper L'_Q for DC-SQUID. However, Reference 14 follows the idea of Ref. 11 to use AC microwave signals at the angular frequency $\omega_\pm = (\Delta_1^{eff} \pm \Delta_2^{eff})/\hbar$ to couple qubits 1 and 2. Why can the modulated AC signal in the coupling term $J_{12}^{eff}(t)$ achieve a constant transition between two states? Because there exist terms of the angular frequency components $\omega_\pm$ in the interaction representation in my opinion.

The authors in Ref. 14 argue that the DC-SQUID-coupling scheme employing a large I_b contradicts the optimal current bias condition[10,13] for the single qubit which requires $\partial\Delta\gamma_q/\partial I_b = 0$ (see the measurement section) to effectively decouple the flux qubit from its measuring circuit and optimally cancel out the noises from I_b to the first order. Ideally, DC-SQUID goes at the optimal point with $I_b = 0$; due to 4% asymmetry of its two junctions in fabrications, Ref. 10 takes the optimal I_b^* as $I_b^* = 180 \pm 20nA$ but still much less than the switching current $I_C \sim 1\mu A$ of DC-SQUID. However, it is not obvious why qubit 3 holding a large loop current cannot trap some noises to impact qubits 1 and 2 in their scheme. Without further theoretical analysis, I think, the reason may be that we never measure qubit 3 for any quantum informations. Since the measurement is always a decoherent procedure because it projects the quantum states into classical ones, the DC-SQUID coupling scheme has a higher possibility to couple the qubits to the measuring environment, causing their decoherence.

Finally, the theoretical schemes are presented completely. I agree with the authors' comments on the third-qubit scheme: taking the flux qubits as tunable coupling elements makes the circuits easier to fabricate in compatible technologies; all magnetic controls and frequency multiplexed(assuming different splittings) requires a minimal number of microwave lines; it is crucial for this kind of coupling scheme that optimal points exists and the effective coupling at DC regime can be set to zero if desired.

B. Experimental results

First af all, I find that Ref. 15 utilizes the new designed and more symmetric flux qubit shown in fig. 2(d) compared to fig .2(c). It is because in a given I_b the latter one reduces the circulating current in the loop of DC-SQUID into zero ideally and, thus, couples less noises to the flux qubit, which is still a issue on how to select the optimal point for I_b.[8]

Different schemes lead to different realizations for Refs. 12 and 15(See fig. 4). In the former one, DC-SQUID functions as both the measuring and effective coupling elements, so two bias lines are included to independently control qubits 1 and 2. The latter one, only utilizes single uniform flux bias for qubits 1,2 and 3, controls the accuracy of lithography to make sure of $\Phi_1 \simeq \Phi_2$ whereas Φ_3 is deliberately offset to generate a finite coupling for qubits 1 and 2. Its DC-SQUID besides as a measuring device also fine-tunes qubits 1 and 2 to be at the opitmal point. It seems that the latter one's design is of less metal lines, simple and robust; yet, I am not sure of its flexibilities if we design a system consisting of more flux qubits. Both of them only fabricate one DC-SQUID, so they cannot measure qubits 1 and 2 individually without destroying the other qubit's quantum informations and always obtain the informations of the four-level quantum system shown in fig.4(b)(B).

Generally, the evidences of the coupling betwne qubits 1 and 2 are that there are direct transitions of $\mid 10\rangle \leftrightarrow \mid 01\rangle$ and $\mid 00\rangle \leftrightarrow \mid 11\rangle$. Reference 12 carefully tunes the flux biases of almost identical qubits 1 and 2 to find a degenerate point for $\mid 10\rangle$ and $\mid 01\rangle$, the cross point in the first subfigure of fig. 5. At this degenerate point $\mid 10\rangle$ and $\mid 01\rangle$ forms a new two-level system and the tunnable couplings, if existing, lead to tunnable fine splitting structures shown in the last three figures in fig. 5. Reference 15 focuses on the other transtion $\mid 00\rangle \leftrightarrow \mid 11\rangle$. The spectra in fig. 6 shows that they fabricate qubits 1 and 2 of different sizes and the observed line $(\Delta_1 + \Delta_2)/h$ only indicates there is a coupling between qubits 1 and 2. Further proofs are given in the last seven figures in fig. 6 showing dynamics of the transitions between different states. Figures from A to D demonstrate single qubit operations. Figures from E to G show the transition runs faster if a AC signal of a larger amplitude is applied, with a maximum speed of 23.2MHz, indicating a tunable coupling. I think the results also suggest that we should enlarge the coherent time so that the transition curves cannot decay as fast as $\sim$300ns.

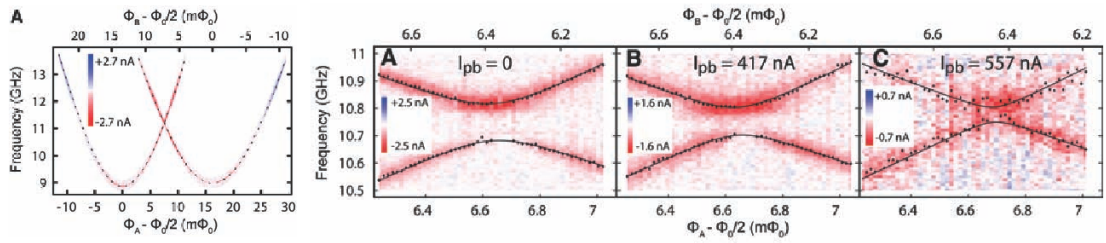

FIG. 5: Experimental results in Ref. 12

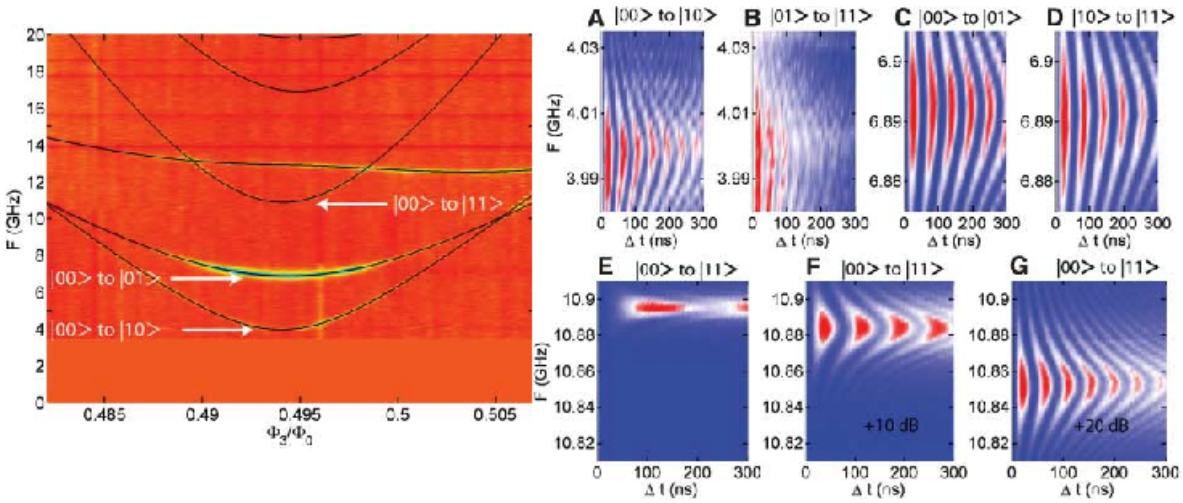

FIG. 6: Experimental results in Ref. 15

IV. CONCLUSION

In this report I present some introductions to flux qubits and coherent tunable coupling between them. Flux qubit as a superconducting circuit dominated by quantum mechanics can be treated as a two-level quantum system with a proper set of parameters. To minimize the impacts of the low frequency noises flux qubit may work better in the optimal point $\Phi_{ext} = \frac{1}{2}\Phi_0$. Fabrications of flux qubits show high flexibilities in design which still requires amounts of design skills to cope with them, e.g., for auxiliary circuits. Flux qubit is usually measured using a DC-SQUID which can detect its small loop current. Finally, I try my best to understand and interpret two coherent tunable coupling schemes and their realizations:

coupling two flux qubits with a DC-SQUID or a third flux qubit.

---

[1] J. J. ToppariCorresponding, K. Hansen, N. Kim, M. T. Savolainen, L. Taskinen and J. P. Pekola. *Physica C*, **352**, 177 (2001).

[2] D. Vion, A. Aassime, A. Cottet, P. Joyez, H. Pothier, C. Urbina, D. Esteve, M. H. Devoretd. *Science*, **296**, 886 (2002).

[3] T. P. Orlando, J. E. Mooij, Lin Tian, C. H van der Wal, L. S. Levitov, S. Lloyd, and J. J. Mazo. *Phys. Rev. B*, **60**, 15398 (1999).

[4] J. E. Mooij, T. P. Orlando, L. Levitov, Lin Tian, Caspar H. van der Wal, Seth Lloyd. *Science*, **285**, 1036 (1999).

[5] Caspar H. van der Wal, A.C.J. ter Haar, F. K. Wilhelm, R. N. Schouten, C.J.P.M. Harmans, T.P. Orlando, S. Lloyd, J.E. Mooij. *Science*, **290**, 773 (2000).

[6] I. Chiorescu, Y. Nakamura, C.J.P.M. Harmans, J.E. Mooij. *Science*, **299**, 1869 (2003).

[7] B. L. T. Plourde, J. Zhang, K. B. Whaley, F. K. Wilhelm, T. L. Robertson, T. Hime, S. Linzen, P. A. Reichardt, C.-E. Wu, and John Clarke. *Phys. Rev. B*, **70**, 140501(R) (2004).

[8] G. Burkard, D. P. DiVincenzo, P. Bertet, I. Chiorescu, and J.E. Mooij. *Phys. Rev. B*, **71**, 134504 (2005).

[9] G. Ithier, E. Collin, P. Joyez, P.J. Meeson, D. Vion, D. Esteve, F. Chiarello, A. Shnirman, Y. Makhlin, J. Schriefl, and G. Schön. *Phys. Rev. B*, **72**, 134519 (2005).

[10] P. Bertet, I. Chiorescu, G. Burkard, K. Semba, C.J.P.M. Harmans, D.P.DiVincenzo, and J.E.Mooij. *Phys. Rev. Lett.*, **95**, 257002 (2005).

[11] P. Bertet, C. J. P. M. Harmans, and J. E. Mooij. *Phys. Rev. B*, **73**, 064512 (2006).

[12] T. Hime, P. A. Reichardt, B. L. T. Plourde, T. L. Robertson, C.-E. Wu, A. V. Ustinov, John Clarke. *Science*,**314**, 1427 (2006).

[13] F. Yoshihara, K. Harrabi, A.O.Niskanen, Y. Nakamura, and J.S.Tsi. *Phys. Rev. Lett.*, *Phys. Rev. Lett.*, **97**, 167001 (2006).

[14] A. O. Niskanen, Y. Nakamura, and J.S. Tsai. *Phys. Rev. B*, **73**, 094506 (2006).

[15] A. O. Niskanen, K. Harrabi, F. Yoshihara, Y. Nakamura, S. Lloyd, and J.S. Tsai. *Science*, **316**, 723 (2007).

[16] Figure obtained in "http://qt.tn.tudelft.nl/research/fluxqubit/" which citing Ref. 4.

[17] R. C. Jaklevic, John Lambe, A. H. Silver, and J. E. Mercereau. *Phys. Rev. Lett*, **12**, 159 (1964).